Ocean Engineering 297 (2024) 117006

Contents lists available at ScienceDirect

Ocean Engineering

journal homepage: www.elsevier.com/locate/oceaneng

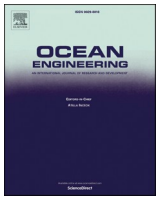

Research paper

Floating-state calculation method based on tetrahedral meshing

Xiao Liu, Quan Zhou *, Lei Xu

School of Civil Engineering and Transportation, South China University of Technology, Guangzhou, 510640, China

ARTICLE INFO

Keywords:
Floating state
Tetrahedral element
Hydrostatic property

ABSTRACT

Flotation and stability calculations are key components of vessel design and construction. The field of floating-state calculations has a long research history. However, certain difficulties remain in practice, particularly for multihull vessels. In this study, we devised a new method called the tetrahedral mesh method (TMM) for evaluating the flotation and stability of multihull vessels, which is more convenient than the 3D surface method. The TMM is implemented in three steps. First, the 3D floating body is discretized into a number of tetrahedral elements. Second, the hydrostatic properties of each tetrahedral element are calculated. Finally, the hydrostatic properties of the entire vessel are evaluated by summing the properties obtained in the second step. By comparing numerical and physical experiments under various working conditions, our algorithm achieved an average deviation of only 3.9%. Furthermore, the restoration curves of the platform at different azimuth angles were also determined using the TMM.

1. Introduction

The flotation and stability of a ship/platform have been evaluated and ensured during the design stage and safety assessment under various loading conditions (Francescutto, 2016; Sequeira and Mann, 2016). There are two fundamental elements for floating-state calculations: buoyancy and gravity. Gravity can be regarded as a constant. Buoyancy is variable, and its calculation methods include the following: (1) section method, (2) 3D surface element method, and (3) 3D body-element method.

The classical section method (Biran, 2003) is particularly suitable for monohulls but not for multihull vessels.

The 3D surface element method has been proposed to solve the flotation problem of multihull vessels (Radwan, 1983; Rabien, 1985; Witz and Patel, 1985; Schalck and Baatrup, 1990; van Santen, 1986). The usual practice in such a method is to model the surface of a floating body using many 3D triangular elements. The hydrostatic properties can then be derived by pressure integration of these triangular elements. There are three difficulties in applying the 3D surface method. As shown in Fig. 1, the normals of all the surface elements must be directed outward from the floating body and carefully assigned one by one. Clearly, a normal assignment is tedious. The second difficulty is that the hull surface must be remeshed when the cabin of the vessel is flooded (see Fig. 2). Finally, duplicate faces between the convex bodies must be deleted. Consider the semi-submersible vessel and cylindrical caisson shown in Fig. 3a as examples. Two duplicate circular faces existed between the two convex bodies. One of the circular faces must be removed to prevent the same pressure integration from being performed a second time (see Fig. 3b).

In addition to the pressure integration method based on 3D surfaces, some researchers (Calabrese et al., 2012, 2015; Zhang and Xie, 2023) used the finite element method (FEM) to evaluate the equilibrium point of a ship. They calculated the hydrostatic properties using the graphics engines of FEM tools, such as ANSYS, MSC, and ABAQUS. However, some difficulties remain in practice when calculating floating state for multihull vessels.

This paper presents a double-iteration method based on solid 3D tetrahedral meshing, which simulates the heaving and rotational motion of a floating body by inner and outer iterations, respectively.

The flotation of the platform was investigated under three loading conditions: heel, trim, and arbitrary inclination. Through a comparison between the numerical and experimental results, it was verified that the proposed method has a clear physical meaning and is more suitable for flotation calculations for multihull vessels.

2. Geometric characteristics of the tetrahedron

The floating body can be modeled as 3D tetrahedral elements using FEM tools such as MSC, ANSYS, and ABAQUS. Fig. 4 shows the tetrahedral mesh grid of the fuel-supply ship.

* Corresponding author.
E-mail address: zhou_q1999@qq.com (Q. Zhou).

https://doi.org/10.1016/j.oceaneng.2024.117006
Received 5 September 2023; Received in revised form 1 February 2024; Accepted 1 February 2024

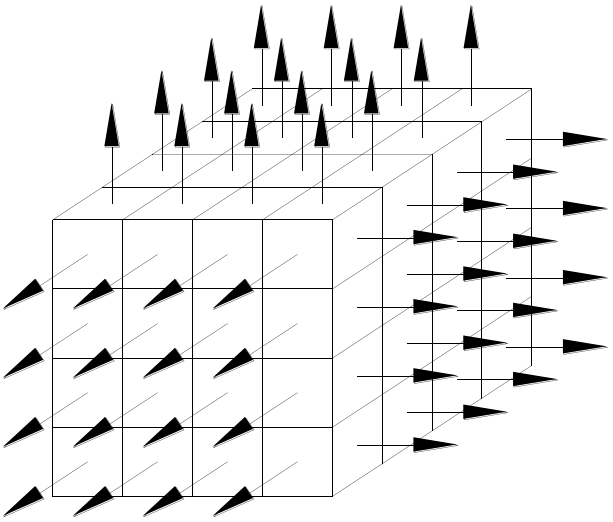

Fig. 1. Surface elements for a box-shaped floating body.

Each tetrahedron (see Fig. 5) consists of four vertices (A, B, C, and D): (x_A, y_A, z_A), (x_B, y_B, z_B), (x_C, y_C, z_C), and (x_D, y_D, z_D).

The volume of the tetrahedron is

$$V = \frac{1}{6}\begin{vmatrix} x_A - x_D & y_A - y_D & z_A - z_D \\ x_B - x_D & y_B - y_D & z_B - z_D \\ x_C - x_D & y_C - y_D & z_C - z_D \end{vmatrix} \tag{1}$$

and its center coordinates are

$$\begin{cases} x = \dfrac{x_A + x_B + x_C + x_D}{4} \\ y = \dfrac{y_A + y_B + y_C + y_D}{4} \\ z = \dfrac{z_A + z_B + z_C + z_D}{4} \end{cases} \tag{2}$$

3. Hydrostatic properties calculation based on the tetrahedral meshing

Suppose a vessel is meshed into n tetrahedral elements. Taking one tetrahedron *tet_i* as an example ($i = 1,2, \ldots n$, where n is the number of

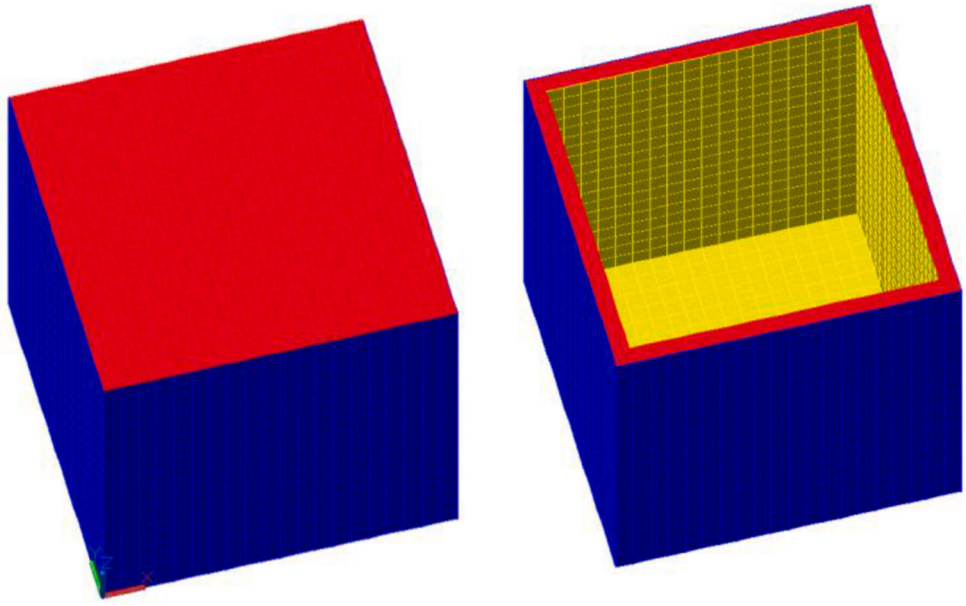

(a) Surface mesh (b) Surface mesh after one cabin is flooded

Fig. 2. Regenerated surface elements.

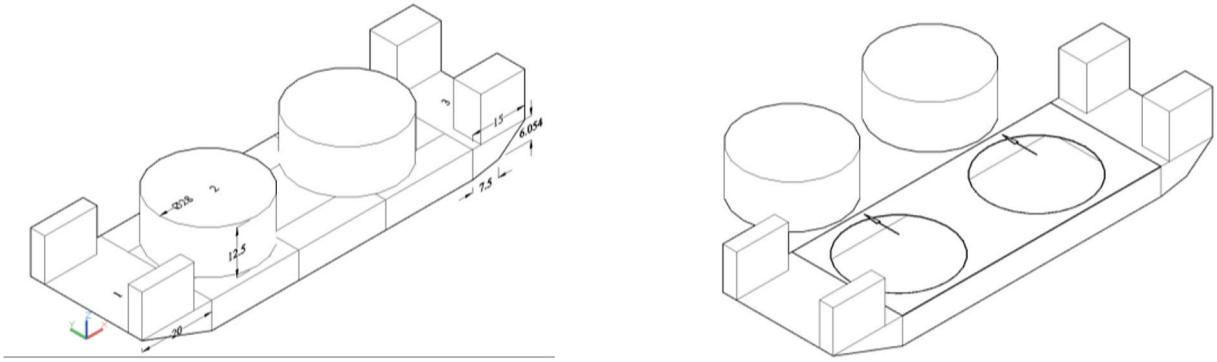

(a) Semi-submersible vessel and cylindrical caisson (b) Common contact surfaces between vessel and caisserias

Fig. 3. Common contact surfaces between two convex bodies.

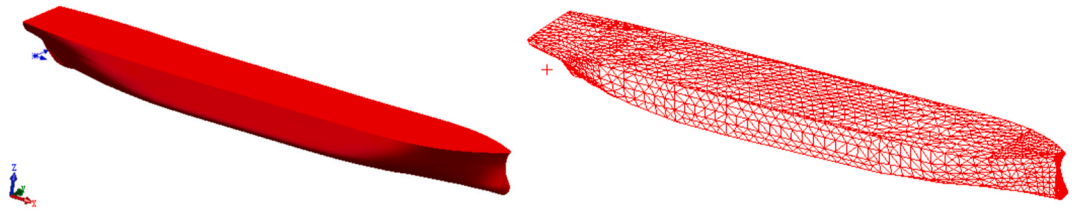

(a) Solid model (b) Tetrahedral mesh model

Fig. 4. Tetrahedral mesh of a fuel-supply ship.

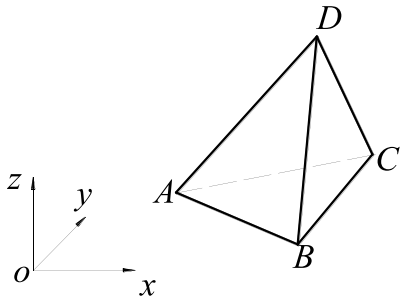

Fig. 5. Tetrahedron.

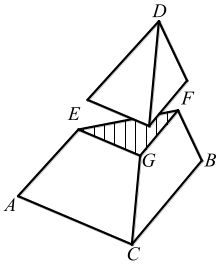

Fig. 6. One vertex (D) above the water.

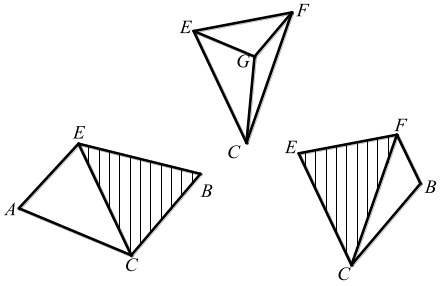

Fig. 7. Sub-tetrahedrons under water.

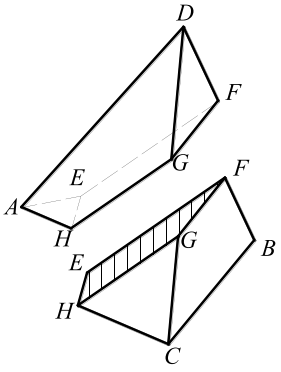

Fig. 8. Two vertices (A and D) above the water.

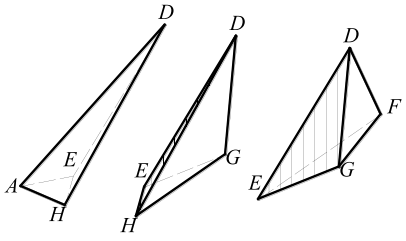

Fig. 9. Sub-tetrahedrons above the water.

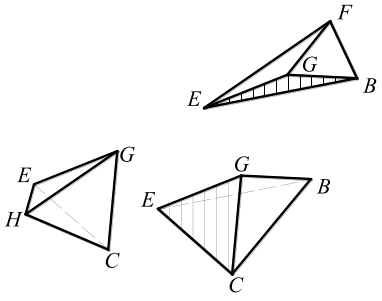

Fig. 10. Sub-tetrahedrons under the water.

tetrahedral elements), its four vertices are classified into two groups by the water plane (WP). Some vertices are above the WP, whereas others are underwater. There are five possible relationships between the vertices and WP.

(1) None of the vertices are above the WP. The volume *is* $v_i = v\_ABCD$.
(2) One vertex is located on the positive side of the WP. The WP cuts the three edges of the tetrahedron at three points (E, F, and G) (see Fig. 6). Point D is on the positive side of the WP, and the other three points (A, B, and C) are underwater. Hence, the original tetrahedron can be divided into four sub-tetrahedrons: DEFG is above the water, and EABC, GEFC, and FEBC are underwater (see Fig. 7). Volume $v_i = v\_EABC + v\_GEFC + v\_FEBC$.
(3) Two vertices are located on the positive side of WP. The WP cuts the four edges of the tetrahedron at four points: E, F, G, and H (see Fig. 8). Points D and A are located on the positive side of WP. The other two points (B and C) are underwater. The original tetrahedron can be regarded as a combination of six sub-tetrahedrons:

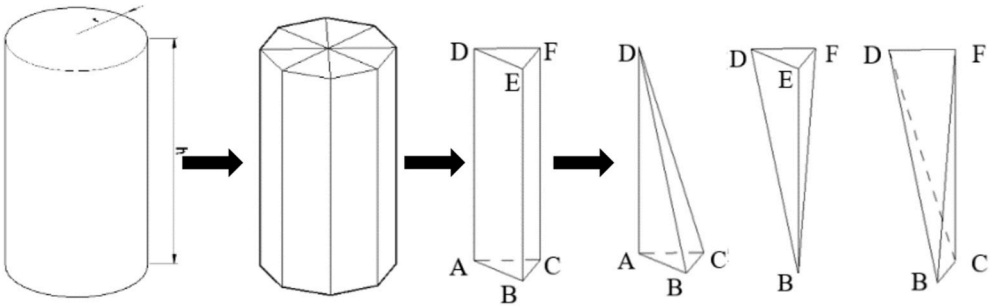

Fig. 11. Schematic of a cylinder and triangular prism divided into tetrahedra.

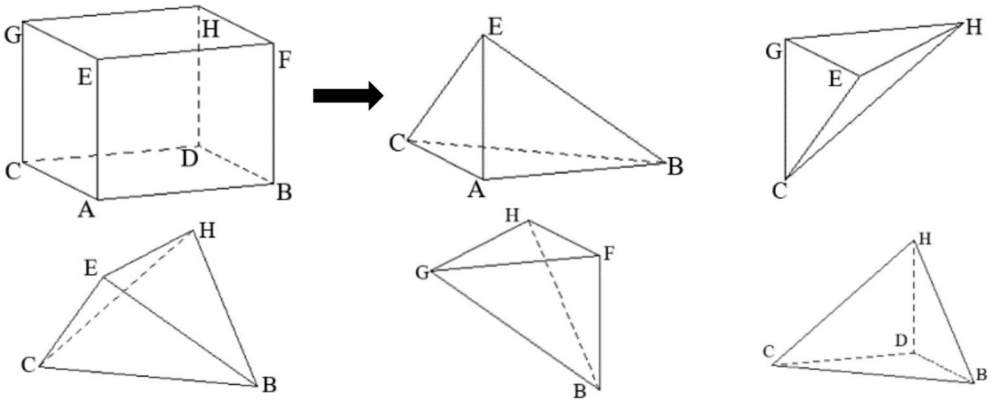

Fig. 12. Schematic of cuboid divided into tetrahedra.

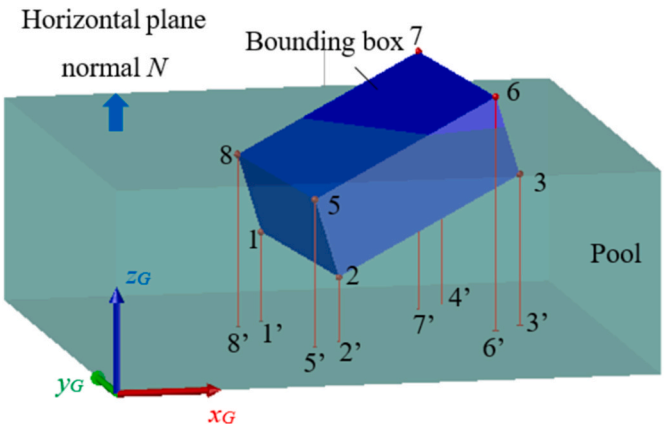

Fig. 13. Bounding box of floating body.

DAEH, DEGH, and DEFG are above water (see Fig. 9), and CHGE, GEBC, and BGFE are underwater (see Fig. 10). Volume v_i = *v_CHGE* + *v_GEBC* + *v_ BGFE*.

(4) Three vertices are located on the positive side of WP. Volume v_i = *v_DEFG*.

(5) All vertices are located on the positive side of the WP. Volume v_i = 0.

So, the displacement of the entire vessel is

$$V = \sum_{i=1}^{n} v_i \tag{3}$$

and its center coordinates are

$$x_c = \frac{\sum_{i=1}^{n} v_i x_i}{V}, y_c = \frac{\sum_{i=1}^{n} v_i y_i}{V}, z_c = \frac{\sum_{i=1}^{n} v_i z_i}{V} \tag{4}$$

Figs. 11 and 12 show the procedures for dividing the cylinder, triangular prism, and hexahedron into tetrahedral elements. A cylinder can be divided into multiple triangular prisms, and then these triangular prisms are divided into tetrahedral elements. For example, triangular prism ABCDEF can be divided into three tetrahedra: ABCD, BDEF, and BCDF. The hexahedron ABCDEFGH can be divided into the following tetrahedra: ABCE, CEGH, BCEH, BFGH, and BCDH.

4. Double-iteration method

The static motion behavior of the vessel includes two parts: a heaving motion along the vertical direction and a rotational motion in any direction. In this paper, a tetrahedral mesh method (TMM) is proposed to simulate these two motions.

4.1. Internal iteration (simulates heaving motion)

Generally, a floating body simultaneously performs heaving and rotational motions. For simplicity, we consider only the heaving motion. In other words, the normal of WP (*N*) is a previously given constant, and the floating body only performs a heaving motion.

As shown in Fig. 13, the bounding box of the floating body has eight vertices whose heights from the bottom of the pool are

$$h_i = lx_i + my_i + nz_i\ ,\ i = 1,2,\ldots,8 \tag{5}$$

Where *l*, *m*, and *n* are the cosine values of the angles between *N* and the *x*, *y*, and *z* axes of the local coordinate system of the floating body, respectively.

Vertex 2 has the lowest (h_2 is the minimum value), and vertex 7 has the highest (h_7 is the maximum) value.

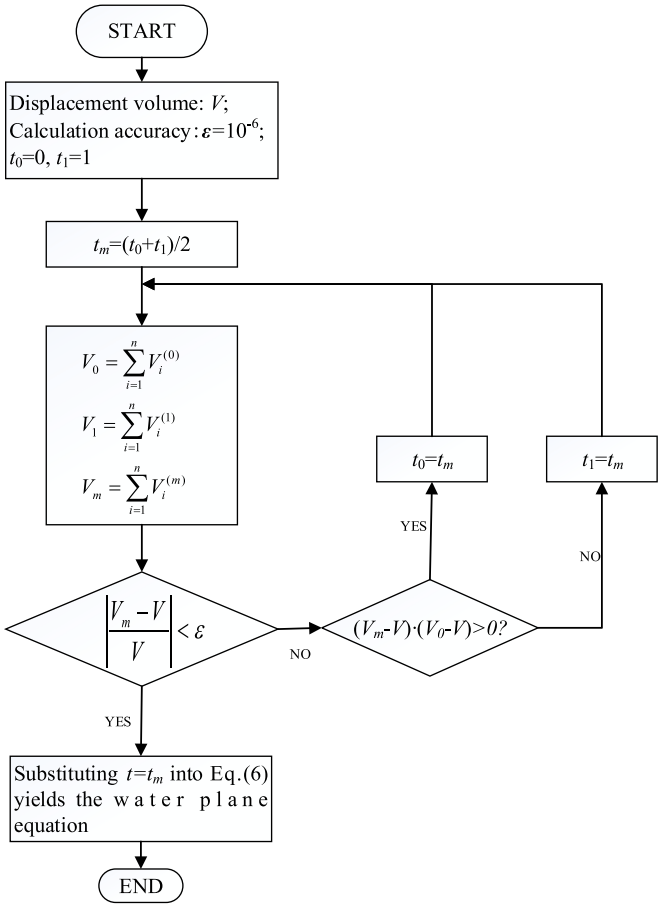

Fig. 14. Logical flow of inner iterative method (simulation of the heaving motion of floating body).

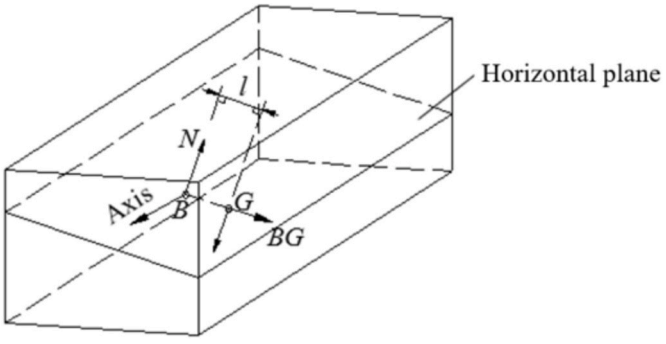

Fig. 15. Rotating shaft of the floating body.

When the WP passes through vertex 2, the displacement volume V is 0, whereas when the WP passes through vertex 7, V reaches the maximum value, which means that the vessel has sunk. Generally, WP passes through point v_t (x_t, y_t, z_t), which must lie between vertices 2 and 7. Therefore, the coordinates of v_t can be described as follows:

$$\begin{cases} x_t = x_0 + t(x_1 - x_0) \\ y_t = y_0 + t(y_1 - y_0) \\ z_t = z_0 + t(z_1 - z_0) \end{cases} \tag{6}$$

for $0 \le t \le 1$.

We used the bisection method to find t, then substituted it into Eq. (6) to obtain the coordinates of v_t. Thus, the WP equation can be obtained as

$$A \bullet (x\text{-}x_t) + B \bullet (y\text{-}y_t) + C \bullet (z\text{-}z_t) = 0 \tag{7}$$

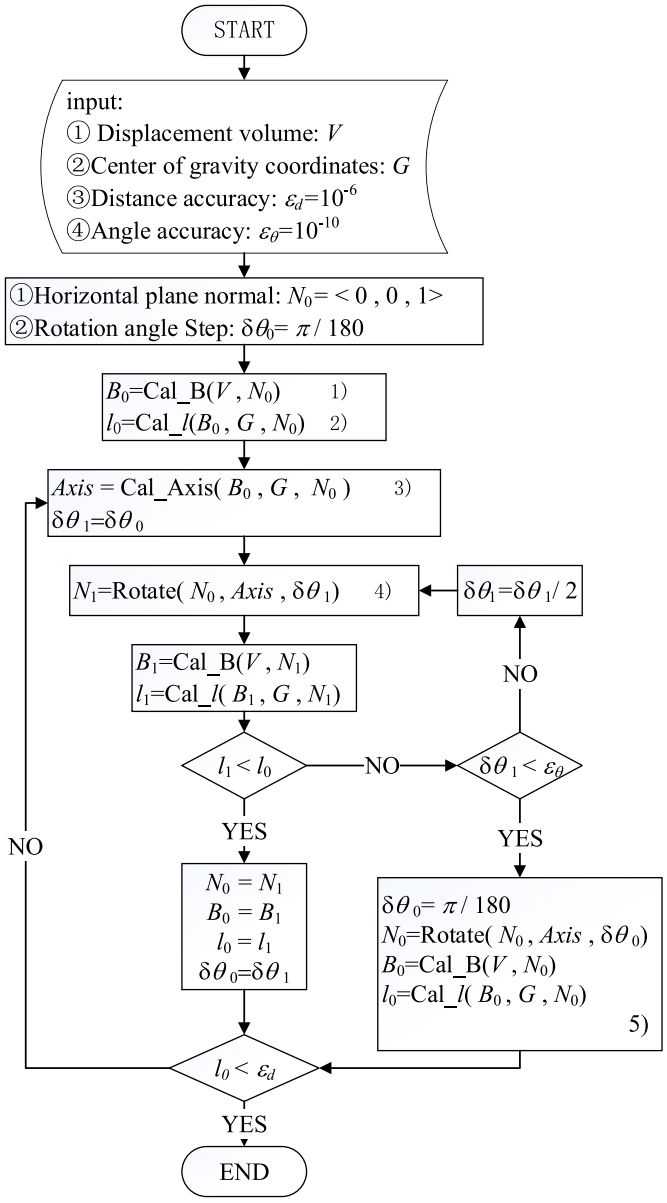

Fig. 16. Flowchart of outer iteration (simulating rotation of the floating body).

Rewritten as:

$$Ax + By + Cz + D = 0 \tag{8}$$

where A, B, C are the three components of N in the global coordinate system.

$$D = -(Ax_0 + By_0 + Cz_0) \tag{9}$$

The corresponding flowchart of *internal iteration* is shown in Fig. 14.

4.2. Outer iteration (simulates rotational motion)

Using the internal iteration method, the buoyancy of the floating body is equal to the weight. However, the gravity line does not necessarily coincide with the buoyancy line. As shown in Fig. 15, the line of buoyancy passes through the floating center B in the same direction as the normal N of WP; the gravitational line passes through the center of gravity G in the opposite direction to N. Assume l as the distance between the buoyancy line and gravity line, if $l \neq 0$, N will rotate around Axis, as shown in Fig. 15 (supposing the floating body remain

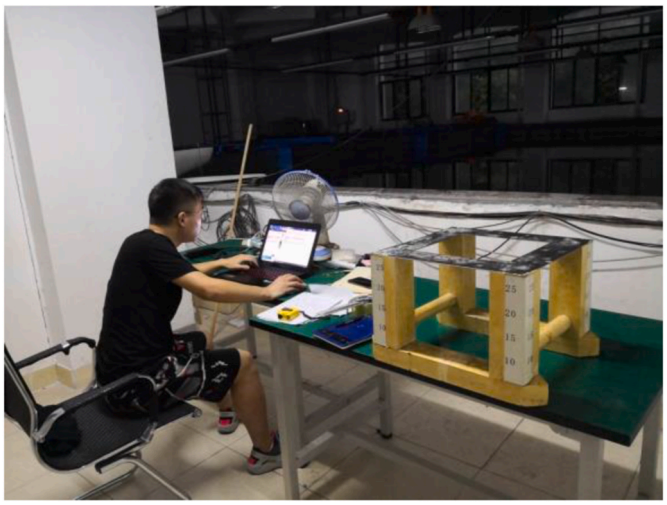

Fig. 17. Experiment environment.

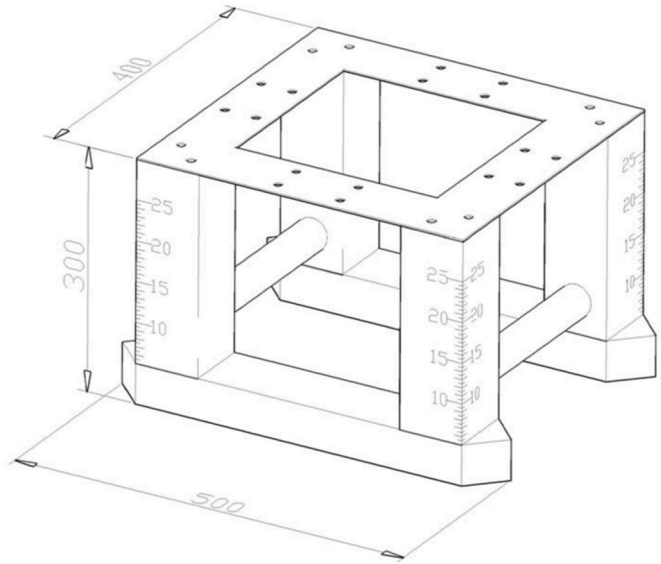

Fig. 18. Model of the semi-submersible platform.

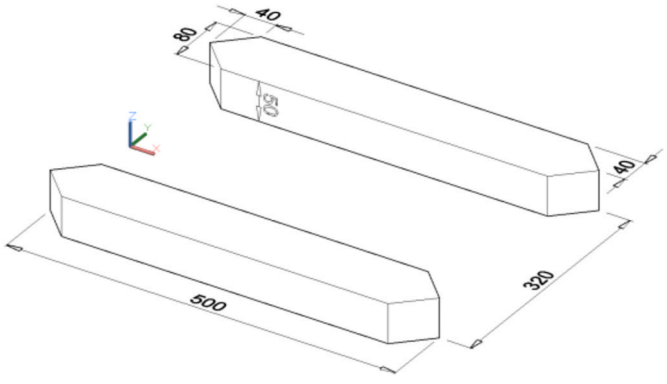

Fig. 19. Parallel floating structure dimensions.

motionless). The Axis can be determined based on the right-handed spiral rule.

$$\text{Axis} = BG \otimes N \tag{10}$$

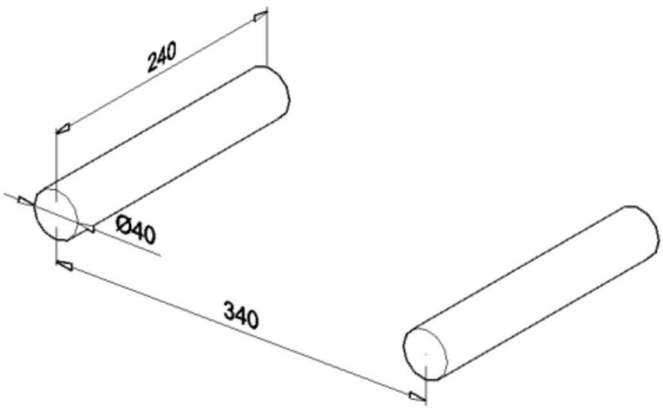

Fig. 20. Transversal cylinders.

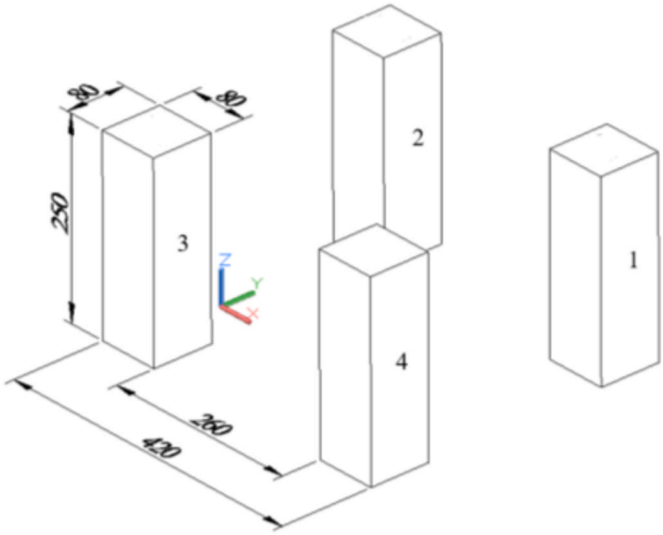

Fig. 21. Vertical columns.

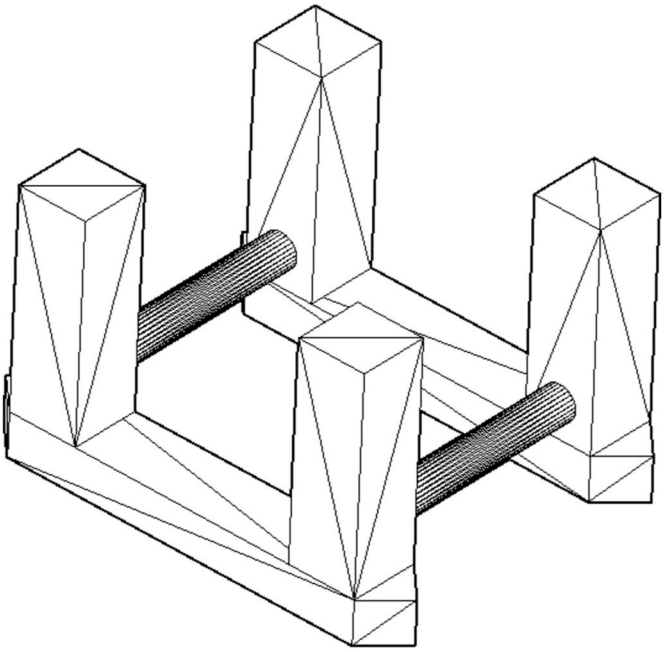

Fig. 22. The TMM model of the semi-submersible platform.

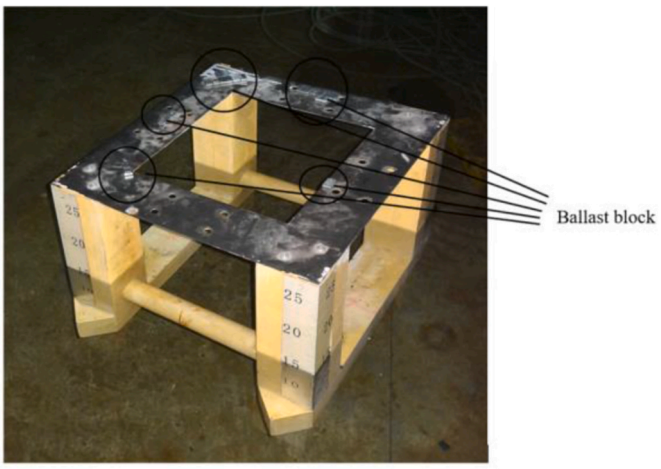

Fig. 23. Floating on even keel.

Suppose the floating body remains upright at the beginning, and its gravity is equal to buoyancy. If the lines of gravity and buoyancy do not coincide, the moment formed by buoyancy and gravity drives the floating body to rotate. For convenience, it is assumed that the floating body remains still, and the normal N (see Fig. 15) of WP rotates around the Axis in equation (10), which results in a new normal direction N'. Then the floating body will rise or sink along N' as described by the inner iterative method in Fig. 14. The floating center B moves to the new location B', and distance l is reduced accordingly. As long as $l \neq 0$, N' will continue to rotate and l decreases further, and so on until $l = 0$ (or less than the specified error). The flowchart in Fig. 16 illustrates this process.

1) Specify the displacement volume V and normal direction N_0 of the WP, and find the WP equation using the inner iterative method (see Fig. 14). Then, the displacement volume v_i and buoyancy center B_i of each tetrahedron can be calculated by analyzing the relationship between each tetrahedron and WP (see Fig. 6−10). Finally, calculate the center of floating body B_0 by equation (4).
2) Specify N_0 (the normal of WP), calculate the distance l_0 between the buoyancy line and the gravity line.
3) Calculate the floating body rotation axis (Axis $= B_0G \otimes N_0$), according to the floating center B_0, the center of gravity G, and WP normal N_0.
4) The new WP normal N_1 could be produced by rotating N_0 by $\delta\theta_1$ around axis obtained in the previous step (supposing that the floating body is motionless and N_0 is rotatable).
5) In some special conditions, no matter how small the rotation angle $\delta\theta_1$ is, the distance between the lines of gravity and buoyancy cannot be reduced. One reason for this phenomenon is that the center of gravity of the vessel becomes too high because of overloading, causing the floating body to be capsized. In this case, the floating body will be forced to rotate around the axis by 1°.

5. Numerical examples

5.1. Experimental model

We conducted a floating test on a model of a semi-submersible platform in an experimental pool (Fig. 17). The principal dimensions of the model are depicted in Fig. 18.

Length L = 500 mm, Light-load weight $M = 6.91$ kg,
Beam $B = 400$ mm, Draft $d = 153$ mm,
Depth $D = 300$ mm, and Height of gravity center Zg = 152 mm.

Its main components include two parallel floating structures (each consisting of one cuboid and two triangular prisms) (Fig. 19), two transversal cylinders (Fig. 20), and four vertical columns (Fig. 21). The TMM model is shown in Fig. 22.

Owing to production errors, some ballast blocks were added to the top of the model to keep it floating on the even keel before the floating experiments were conducted (see Fig. 23).

Three preparation steps were performed: 1. Measurement of the lightweight of the model, including the ballast blocks, 2. Measurement of the center of gravity of the model, and 3. Measurement of the sizes and weights of the load blocks (Fig. 24).

Table 1
The gravity center of the assembly (load block + light model).

	Gravity center of the load block[a]/mm			Gravity center of the assembly/mm		
	x	*y*	*z*	*x*	*y*	*z*
Heel	236	130	303	250	1	153
Trim	110	1	303	249	0	153
Diagonal inclination	100	−149	303	249	−1	153

[a] Note: Mass of the load block was 0.06 kg.

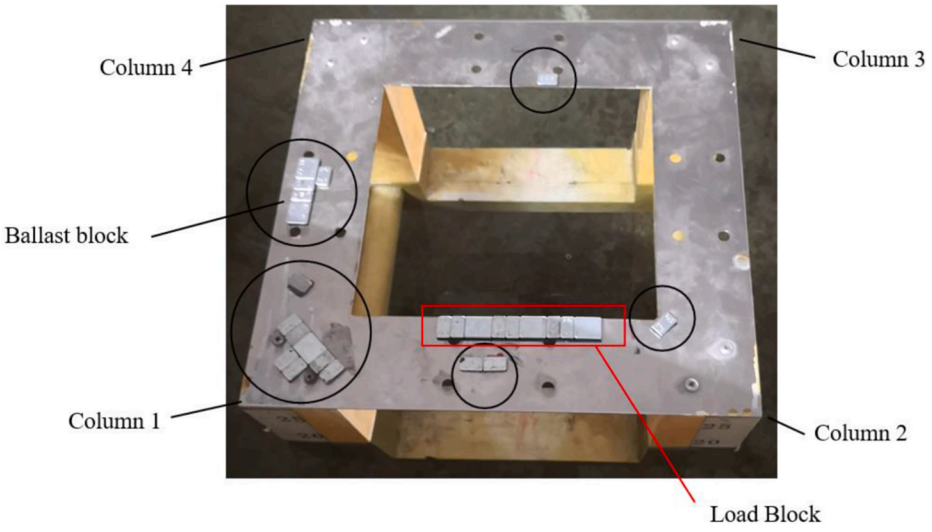

Fig. 24. Ballast and load arrangement on the top of model (heeling).

Table 2
Model data of heel—Heel.txt.

Volume of Displacement = 6.97e6	120,-120,50	380,200,300
Gra_Pt.x = 250	120,-200,50	Hexahedron
Gra_Pt.y = 1	40,-200,50	380,-120,50
Gra_Pt.z = 153	40,-120,300	460,-120,50
Hexahedron	120,-120,300	460,-200,50
40,120,50	120,-200,300	380,-200,50
120,120,50	40,-200,300	380,-120,300
120,200,50	Hexahedron	460,-120,300
40,200,50	380,120,50	460,-200,300
40,120,300	460,120,50	380,-200,300
120,120,300	460,200,50	Hexahedron
120,200,300	380,200,50	40,200,0
40,200,300	380,120,300	40,120,0
Hexahedron	460,120,300	40,120,50
40,-120,50	460,200,300	40,200,50
460,200,0	460,200,0	Cylinder
460,120,0	460,120,50	420,120,90
460,120,50	500,160,50	20
460,200,50	460,200,50	420,-120,90
Hexahedron	TrianglePrism	20
40,-200,0	0,-160,0	###
40,-120,0	40,-120,0	FourPillars.txt
40,-120,50	40,-200,0	
40,-200,50	0,-160,50	
460,-200,0	40,-120,50	
460,-120,0	40,-200,50	#0:
460,-120,50	TrianglePrism	460,200,0
460,-200,50	460,-120,0	460,200,300
TrianglePrism	500,-160,0	#1:
0,160,0	460,-200,0	40,200,0
40,120,0	460,-120,50	40,200,300
40,200,0	500,-160,50	#2:
0,160,50	460,-200,50	40,-200,0
40,120,50	Cylinder	40,-200,300
40,200,50	80,120,90	#3:
TrianglePrism	20	460,-200,0
460,120,0	80,-120,90	460,-200,300
500,160,0	20	#end

5.2. Experimental process

Experiments were performed under three load cases (heel, trim, and diagonal inclinations) by placing the load block at different positions on top of the model (see Table 1). The details of body meshing are listed in Table 2.

The TMM program could be downloaded through: "www.huagongchuanhai.cn/tetrahedron/TMM.zip."

The experimental and numerical draft values for all the columns are listed in Table 3. The maximum deviation between the experimental and numerical values was 10.4%, the minimum was 0.0%, and the average deviation was 3.9%.

From the iteration data and graph (Table 4 and Fig. 25), it can be concluded that the convergence of the algorithm is fine, and all iterations can be completed no more than 18 times.

We also used the TMM to obtain the restoring arm curves of the platform at various azimuths (see Fig. 26 and Table 5). For clear presentation，we plotted the restoring arm curves at four azimuth angles of 0°, 30°, 60°, and 90° (see Fig. 27). It can be seen that the platform has good stability in both directions (longitudinal and lateral inclinations), but poor stability at an azimuth angle of 60°.

6. Conclusion

A new method, the TMM, to calculate the floating state was developed in this study. After describing the TMM algorithm and comparing its numerical solutions with experimental solutions, the following general conclusions were drawn.

(1) The TMM does not need to specify the normal direction for each surface element and does not need to remove the common face between convex bodies. Thus, the TMM is more convenient than the surface element method for model building.

Table 4
Distance between gravity and buoyancy action lines.

Number of iterations	*l*/mm		
	Heel	Trim	Diagonal inclination
1	9.38E-01	7.27E-01	1.25 E+00
2	8.75E-01	4.51E-01	1.10 E+00
3	8.08E-01	1.72E-01	9.73E-01
4	7.36E-01	1.12E-01	8.57E-01
5	6.58E-01	3.12E-02	7.51E-01
6	5.71E-01	4.41E-03	6.51E-01
7	4.76E-01	4.46E-05	5.52E-01
8	3.69E-01	2.49E-05	4.49E-01
9	2.49E-01	0.00 E+00	3.38E-01
10	1.15E-01	0.00 E+00	2.15E-01
11	3.54E-02	0.00 E+00	7.89E-02
12	3.81E-03	0.00 E+00	7.32E-02
13	1.04E-03	0.00 E+00	6.02E-03
14	1.75E-04	0.00 E+00	2.55E-03
15	1.28E-04	0.00 E+00	2.24E-03
16	2.36E-05	0.00 E+00	2.59E-04
17	0.00 E+00	0.00 E+00	5.45E-05
18	0.00 E+00	0.00 E+00	2.32E-05

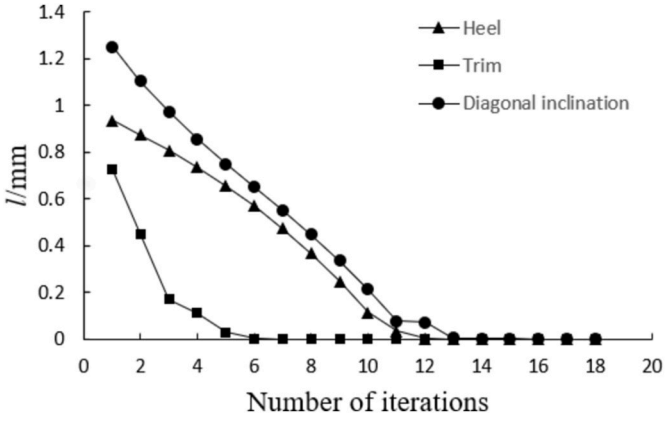

Fig. 25. Curves of distance between gravity and buoyancy action lines.

Table 3
Experimental and numerical values of column drafts.

	Heel			Trim			Diagonal inclination		
	Experimental value /mm	Numerical value /mm	Deviation	Experimental value /mm	Numerical value /mm	Deviation	Experimental value /mm	Numerical value /mm	Deviation
NO.1	190	193	1.6%	136	142	4.2%	95	106	10.4%
NO.2	193	193	0%	172	168	2.4%	126	130	3.1%
NO.3	112	117	4.3%	162	168	3.6%	207	204	1.5%
NO.4	108	117	7.7%	132	142	7.0%	178	180	1.1%

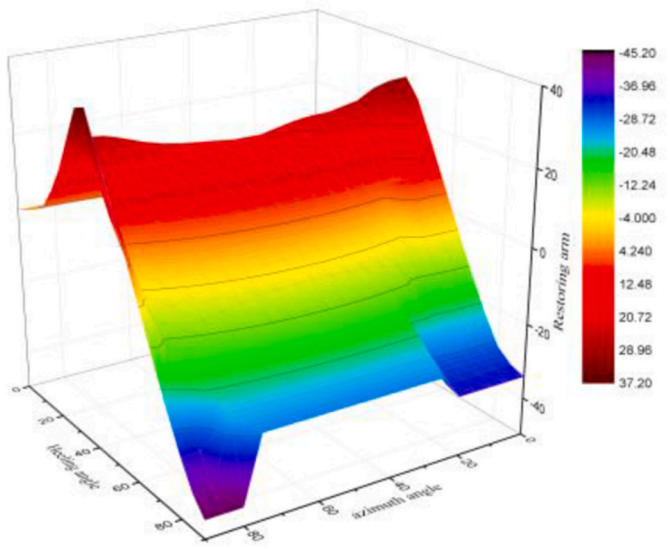

Fig. 26. Restoring arms curves at all azimuth angles.

Table 5
Restoring arms at various azimuths.

	Heeling angle						
	0°	10°	20°	30°	40°	50°	60°
azimuth = 0°	0.00	1.05	3.75	11.68	30.55	17.68	0.69
azimuth = 10°	0.00	1.07	3.84	12.13	29.20	5.59	0.05
azimuth = 20°	0.00	1.15	4.14	13.54	24.02	7.90	−3.75
azimuth = 30°	0.00	1.29	4.70	15.85	20.02	8.51	−2.29
azimuth = 40°	0.00	1.51	5.58	18.14	17.57	8.27	−1.72
azimuth = 50°	0.00	1.82	6.80	19.54	15.99	7.51	−1.92
azimuth = 60°	0.00	2.21	8.31	20.61	14.83	6.26	−2.84
azimuth = 70°	0.00	2.66	9.64	22.79	13.64	4.35	−4.53
azimuth = 80°	0.00	3.04	10.50	26.02	11.71	1.49	−7.05
azimuth = 90°	0.00	3.21	10.97	26.84	37.14	19.50	1.05

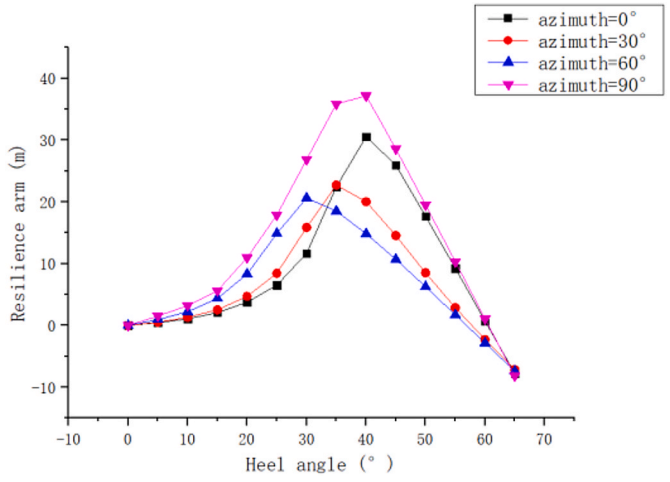

Fig. 27. Restoring arm curves at four azimuth angles (0°, 30°, 60°, and 90°).

(2) A double iterative method was proposed. The internal iteration simulated the heaving motion, and the outer iteration simulated the rotational motion. Therefore, TMM has a clear physical meaning.
(3) A comparison between the TMM and a physical experiment was conducted, which demonstrated the good precision and convergence of the TMM.

CRediT authorship contribution statement

Xiao Liu: Supervision, Software, Project administration, Methodology, Investigation, Funding acquisition, Conceptualization. **Quan Zhou:** Writing – review & editing, Writing – original draft, Visualization, Validation. **Lei Xu** Resources, Formal analysis, Data curation.

Declaration of competing interest

All authors disclosed no relevant relationships.

Data availability

Data will be made available on request.

Acknowledgment

This work was supported by the Department of Industry and Information Technology of the Guangdong Province. Further, it was conducted as 2021 Guangdong Province Special Project for Promoting High-quality Economic Development (Marine Economic Development) Key Project “R&D and Application Demonstration of High-performance Offshore Wind Power Operation and Maintenance Vessels and Core Equipment in the Deep Sea (GDNRC[2021]39)." The authors are grateful to the Department of Industry and Information Technology of Guangdong Province for providing the research funds.

References

Francescutto, A., 2016. Intact stability criteria of ships – past, present and future. J. Ocean Eng. 120, 312–317.
Sequeira, D., Mann, B.P., 2016. Static stability analysis of a floating rectangular prism. In: Proceedings of the ASME Design Engineering Technical Conference.
Biran, A.B., 2003. Ship Hydrostatics and Stability. Elsevier Ltd.
Radwan, A.M., 1983. A different method to evaluate the intact stability of floating structures. Mar. Technol. 20 (1), 21–25.
Rabien, U., 1985. Integrating patch models for hydrostatics. Comput. Aided Geomet. Des. 2, 207–212.
Witz, J.A., Patel, M., 1985. A pressure integration technique for hydrostatic analysis. Transactions of RINA 127, 285–294.
Schalck, S., Baatrup, J., 1990. Hydrostatic stability calculations by pressure integration. Ocean. Eng. 17 (1–2), 155–169.
van Santen, J.A., 1986. Stability calculations for jack-ups and semisubmersibles. In: Proceedings of CADMO. Springer-Verlag, Washington, D.C.
Calabrese, F., Mancarella, L., Zizzari, A.A., Corallo, A., 2012. A FEA-like method for evaluating the ship equilibrium point. IFAC Proc. 9 (1), 115–120.
Calabrese, F., Cataldo, M., De Pascalis, A., et al., 2015. A method for evaluating the ship equilibrium point using 3D meshes developed for embedded device. MTS/IEEE OCEANS 2015 - Genova: Discovering Sustainable Ocean Energy for a New World 1–6.
Zhang, Z., Xie, D., 2023. A mesh insensitive finite element method to compute statical stability curve of floating bodies with arbitrary configurations based on a force-oriented approach. Int. J. Numer. Methods Eng. 124 (7), 1672–1695.